Deep-learning-based Position Control of a Robotic Catheter under Environmental Contact

Di Wu*, Yao Zhang*, Mouloud Ourak, Xuan Thao Ha, Kenan Niu,
Jenny Dankelman and Emmanuel Vander Poorten

***Abstract*— Precise control of robotic catheters remains challenging in interventions. Inherent non-linearities such as hysteresis and external disturbances such as blood flow or contact with the vessel walls have a large impact on the reachable positioning precision. As inaccurate positioning of the catheter tip could lead to tissue damage, controllers that would perform adequately in the presence of hysteresis and environmental contacts would be highly desirable. This paper proposes a method based on multiple Long Short-Term Memory Networks (LSTMs). To this end, a so-called free-space-LSTM (f-LSTM) is trained in order to steer the catheter when it moves in free. Constrained-space-LSTMs (c-LSTMs) are trained to drive the catheter when it is in contact with an obstacle. Based on contact estimation methods, LSTMs are switched. The f-LSTM and c-LSTMs are first tested in free space motion and under constraint situations. The results reveal that LSTMs perform well (RMSE $<$ 0.5 mm) for a steerable robot section with a total length of 77 mm when tested in the same situation where trained. However, when f-LSTM and c-LSTM were tested in an environment different from the one in which they were trained, errors tended to increase. The results highlight the need to exhaustively estimate the contact location and switch between different LSTMs accordingly. The effective working range of a c-LSTM was investigated as well. Experiments showed that a well-trained single c-LSTM could be used effectively in a range of 8.8 mm among the entire length of a steerable catheter section, while maintaining the average tip positioning error below 2 mm in this range.**

I. INTRODUCTION

Coronary artery disease (CAD) forms a threat to humans health worldwide. CAD may cause a variety of symptoms such as chest pain, unusual fatigue, and even sudden death [1]. Catheters, which are long snake-like instruments, are commonly used for treating CAD. Due to their flexible nature, catheters can be inserted via a small incision into the body. Then they can be steered manually by the interventionist through intricate blood vessels, reaching the designated area where they can e.g. widen an artery. When tackling occluded coronaries, this procedure is known as Percutaneous Coronary Intervention (PCI).

Currently, catheters used in interventions are generally passive. They are manually steered by the interventionist. This procedure is skill-intensive. To address this kind of challenge, robotic assistance, which may provide increased precision and enhanced dexterity, is introduced in steering different flexible/continuum surgical tools [2]–[6]. Catheters that incorporates robotic assistance are known as robotic catheters, which could simplify the interventional procedure. Robotics catheters rely on various actuation principles [7]. However, regardless of the adopted actuation method, precise control of robotic catheters remains a challenge as all actuation is affected by inherent non-linearities and external disturbances. Hysteresis is one of the most typical non-linearities that can be found in robotic catheters, leading to a complicated multi-valued relation between the actuation input and the response of the catheters distal tip. If left untackled, hysteresis will lead to inaccurate positioning. This may slow down the PCI procedure, cause perforation of vessel walls or thrombus formation [8]. Past studies proposed deep learning approaches namely a Long Short-Term Memory network (LSTM) to model [9] and compensate [10] for the hysteresis. Previous work focused on steering robotic catheters in free space and showed that good precision could be reached. This paper investigates position control in the presence of both hysteresis and external disturbances.

External disturbances could originate from blood flow or contact with vessel walls. This is a realistic but much more complicated scenario compared to past studies. Due to the deformable and fragile nature of the lumen, precise control of the catheter in such constrained scenario is imperative. A few models for representing the kinematics or/and dynamics of a catheter, or in a broader sense, flexible surgical robots, have been proposed in order to precisely positioning the catheter tip under environmental contacts. A closed-loop position control based on feedback from electromagnetic tracking was introduced in [11]. Qi *et al.* derived a kinematic model for a multi-DOF robotic catheter [12], and implemented a fuzzy-model-based method with feedback from Eletro-Magnetic (EM) trackers [13]. Kesner *et al.* [14] implemented position control of a cardiac catheter by compensating for friction and backlash in the catheter. The *in vivo* experiment showed rms errors below 1.0 mm for valve tracking when operatig under 3D ultrasound image guidance . This work did not take the external disturbances into account. Back *et al.* introduced a model-free tension control approach for catheter steering [15]. However, this approach did not achieved a better performance than the inverse Jacobian method in terms of precision. Xu *et al.* adopted machine learning and proposed three regression methods to model the inverse kinematics of a tendon-driven continuum surgical manipulator [16]. These regression methods were only validated by trajectory following experiments in free space. Yu *et al.* introduced a

*These authors contributed equally to this work.

D. Wu, Y. Zhang, M. Ourak, X. T. Ha, K. Niu and E. Vander Poorten are with the Department of Mechanical Engineering, KU Leuven, Belgium *(Corresponding author: Di Wu, Email: di.wu@kuleuven.be)*

D. Wu and J. Dankelman are with the Faculty of Mechanical, Maritime and Materials Engineering, Delft University of Technology, the Netherlands

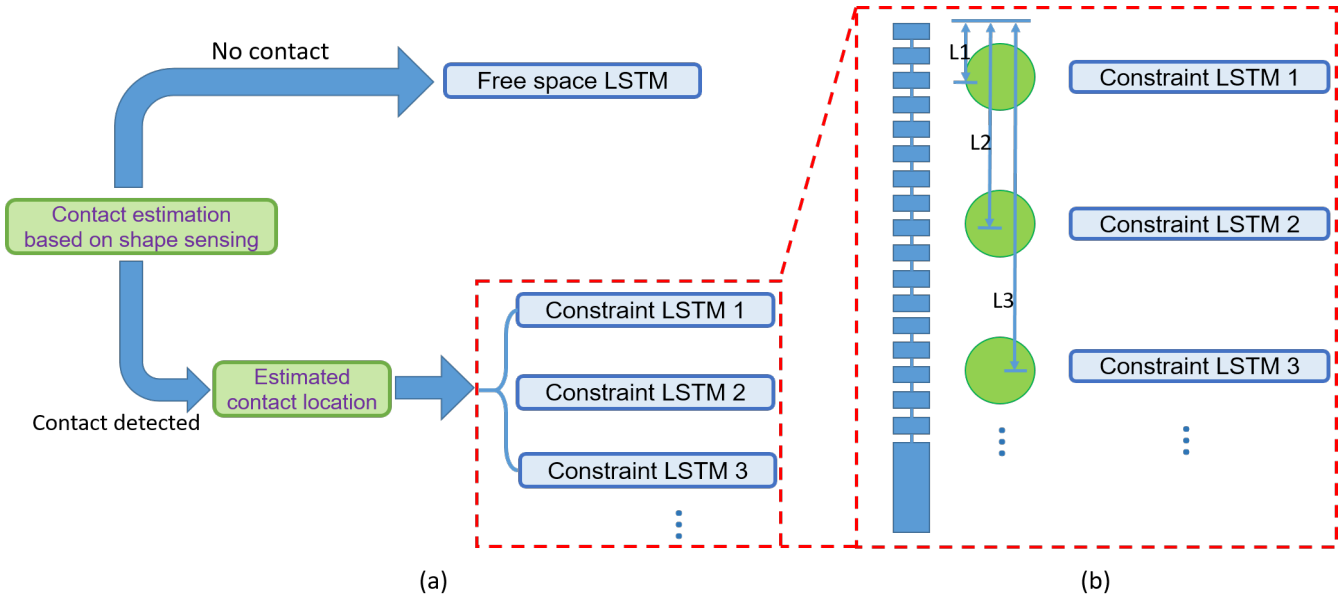

Fig. 1. The proposed framework: (a) based on contact estimation and estimation of contact location, controllers are switched. If no contact with an obstacle is detected, the free-space-LSTM is selected. If a contact is detected, the most appropriate constrained-space-LSTM is selected in line with the estimated contact location; b) the number and the distribution of constrained-space-LSTM ought to be determined based on the required precision.

probabilistic kinematic model based on a Gaussian Mixture Model (GMM) for 3D position control of a catheter [17]. The proposed control method can navigate the catheter tip to follow a desired 3D trajectory in open space and/or in a constrained environment. However, catheter control in constrained environment was only validated in simulation. Moreover, both works, namely [16] and [17], used traditional machine learning methods such as regression and GMM while solving the catheter control problem with deep learning would be interesting to explore. This paper continues our previous research [9] by using deep learning to control the catheter tip to a target position under environmental contact.

The main contributions of this work are: 1) proposing a framework to control robotic catheters both in free space and constrained space; 2) training dedicated LSTM networks based on data collected from free space and constrained space producing f-LSTM and c-LSTM respectively; 3) exploring the performance and generalizability (applicable working range) of f-LSTMs and c-LSTMs; 4) experimental validation on a steerable catheter actuated by artificial muscles. The paper is structured as follows: section II introduces a framework for position control of robotic catheters under environmental contact. Section III presents a catheter system that has been used for experimental validation. The structure and the parameters of the f-LSTM and c-LSTM network as well as the generation of training data are also described in Section III. Section IV describes the designed experiment and the results. Finally, Section V concludes the paper and proposes some future work.

II. Proposed Framework

This paper assumes that an estimation of the location where external contacts are made is available. Readers can refer to works like [18] and [19] where real-time contact estimation based on shape sensing methods e.g. embedded FBG fibers [20], [21] is demonstrated. Based on such knowledge, this paper proposes to switch between various LSTMs depending on various on contact situation. Note that for convenience, no contact or a single contact is assumed, whereas expansions to multiple simultaneous contacts remain for further work.

Figure 1 shows the approach towards training. First, training happens without any obstacle, a f-LSTM is trained for this situation, then different c-LSTMs are trained. For each c-LSTM a single obstacle is positioned at a given distance L_i from the tip of the catheter. Depending on the application a reasonable distribution of L_i's is proposed. That many c-LSTMs will then be trained by commanding the catheter to move against those obstacles and recording the corresponding pressure and displacements. The proposed framework consists of a single f-LSTM and several c-LSTMs (Fig. 1) and a mechanism to switch between them at the appropriate instant of time.

It is noteworthy that in this work, the Fiber Bragg grating (FBG) sensor was not integrated to estimate the contact. A shortcut was taken by deliberately placing the obstacle at a known location. To prove the principle in this work only a single f-LSTM and a single c-LSTM with L_1=38.5 mm (middle point of the catheter, see Fig. 1b) mm was trained. The ability of these LSTMs to control different contact states was investigated and is reported in the following.

III. Catheter System and the LSTM

A. Experimental Setup

The proposed framework is showcased on a one-degree-of-freedom fluidic-driven catheter system shown in Fig. 2. The system features a Pneumatic Artificial Muscle (PAM) integrated off-centered in a 40 mm long flexible 4.4 mm OD Nitinol tube. Notches were made in the Nitinol tube such that catheter is bendable and steerable. PAMs are light-weight, easy-to-fabricate and have a high operational

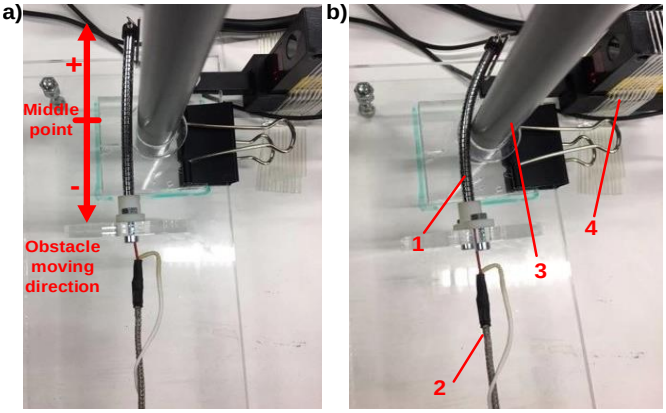

Fig. 2. A bench-top setup for experimental validation: 1. catheter distal segment made of Nitinol; 2. Pneumatic Artificial Muscle; 3. rigid obstacle; 4. laser distance sensor.

bandwidth [22], [23]. However, similar to other catheter actuation methods, they suffer from asymmetric, saturated, rate-dependent hysteresis that needs to be compensated for.

The catheter tip displacement is measured by a laser photoelectric sensor (OADM 12I6460/S35A, Baumer Group, Switzerland) with a sampling frequency of 250 Hz. A Graphical User Interface (GUI) is created based on Labview® to facilitate the experimental procedure.

A hollow tube made of hard plastic was placed to serve as a rigid obstacle in this experiment (Fig. 2). When the catheter is in a straight configuration and an obstacle is simulated, the obstacle is fixed at the midpoint of the catheter length (i.e. the L_1 = 38.5 mm in Fig. 1b), and 9 mm away from the catheter. The catheter first bends in free space and starts to contact the obstacle halfway through its bending action.

B. Training Data Acquisition

It is well-known that deep learning requires abundant data for training. In this work, descending sinusoidal pressure signals described in (1) were used to excite the PAM-driven catheter.

$$p(t) = e^{-\tau t}(A\sin(2\pi f t - \frac{\pi}{2}) + A) \qquad \text{[bar]} \qquad (1)$$

The resulting catheter tip displacement and collected pressure data were used to train the LSTMs. The amplitude A in (1) was set to 1.5 bars. The maximum pressure is 3 bars. Three bars were chosen as the maximum amplitude as this value is close to the maximum operating pressure of this custom-made PAM. In addition, one challenge in hysteresis modeling is the dead zone (in our case around 0.5 bar, see Fig. 3a), in which the catheter tip almost does not react when the pressure increases. Beyond this deadzone, catheter tip displacement correlates better to pressure changes. This confirmed that maximum pressure equals to 3 bars is a generalized case to investigate. With this larger maximum pressure it would not incorporate more information in the training data nor increase the modeling difficulty. The parameter τ regulates the descending speed and was set at 0.05. This value is chosen empirically. A large τ value leads to a fast drop in the sine wave and thus generates insufficient training data, while a small τ value largely increases training time.

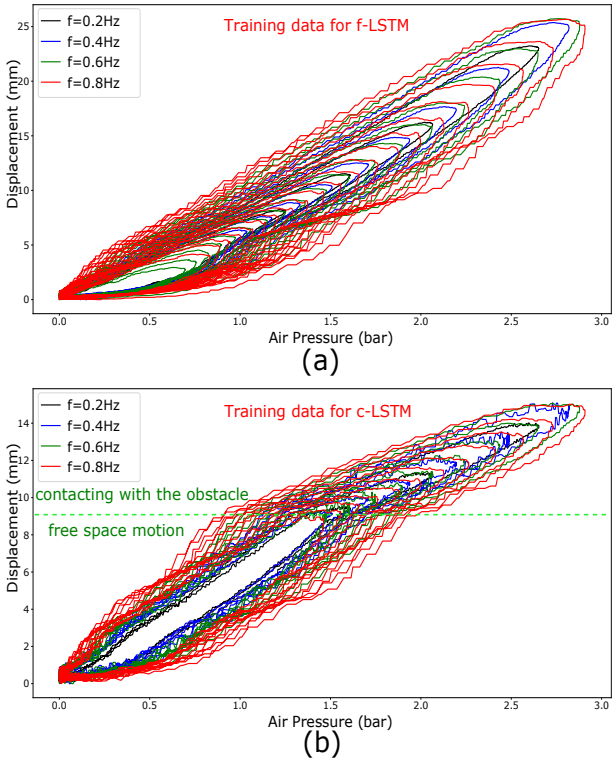

Fig. 3. The training data for the f-LSTM and the c-LSTM: (a) the training data collected in free space under four frequencies from 0.2 to 0.8. (b) training data collected in constrained case. The data that below the green dash line are free space motion, while the data above the green dash line are contacting with the rigid obstacle.

The variable f is the excitation frequency in Hz. The training data was collected under 0.2, 0.4, 0.6, 0.8 Hz. At each τ and f, data were collected in both the presence and absence (i.e. free space motion) of the obstacle. The data collected in free space was used to train the f-LSTM, while the data collected in constrained situation was used to train the c-LSTM. The total number of data points for the f-LSTM and the c-LSTM are 24626 (see Fig. 3a) and 15040 (see Fig. 3b), respectively. Due to the gap between the obstacle and the catheter, the catheter cannot contact the obstacle after several bending loops when being excited with a descending sinusoidal pressure. Since then the training data collection for the c-LSTM is stopped. Therefore, shorter sampling time of the c-LSTM compared to f-LSTM results in less c-LSTM training data on condition that the sampling frequency is the same. The training data collected in free space forms normal rate-dependent hysteresis loops, in which the width of the hysteresis loops expands with increasing frequencies. As visible in Fig. 3b, the data collected in constrained situation can be separated into two parts that are marked by a dashed line. At pressure levels below the dashed line, the catheter has not yet established contacted with the obstacle. Above the dashed line, the catheter is in contact with the obstacle. It can be clearly observed that the inclination of the upper and lower parts differs. However, all of the data shown in Fig. 3b were used to train the c-LSTM.

TABLE I

HYPERPARAMETERS FOR BOTH THE F-LSTM AND THE C-LSTM

	Number of hidden layers	Number of neurons per cell	Activation functions	Optimizer	Loss function	Training-subset /Validation ratio	Batch size	Learning Rate	Epoches
LSTM	4	128	Tanh/Sigmoid	Adam	L2 Loss	70% 30%	16	0.001	100

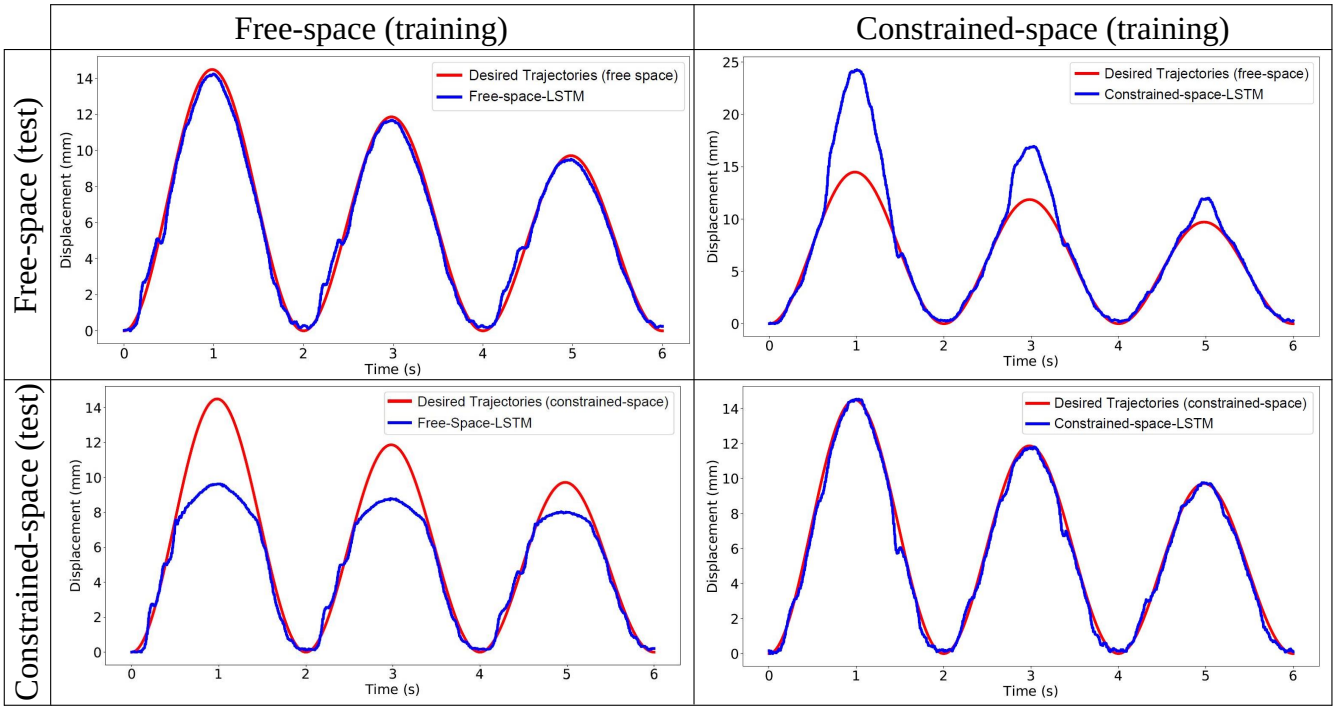

Fig. 4. The performance of the f-LSTM and c-LSTM tested in contact and non-contact situation. Red lines represent the desired trajectories, while the blue lines represent the real trajectories.

C. LSTM

From their origin, LSTMs were proposed as a tool to process sequential information and take historical information into account [24]. It is therefore logical to also consider the use of an LSTM to compensate for the hysteretic behavior, which is typically also associated to a memory-effect and to explore the combination of external disturbances and hysteresis. Note that the hysteresis in this work results not only from the PAM but also from, e.g. friction between different moving parts during bending, flexibility of the pneumatic tube, non-linear behavior of the material used (Nitinol), compressibility of the air, and nonlinearities of pressure valve used. All these factors together determine the resulting hysteresis behavior. Being a data-driven approach an LSTM could approach that considers solely inputs and outputs, could learn all of the above factors.

In this work, the f-LSTM and c-LSTM introduced in section II share the same structure and hyperparameters. A 4-layer stacked LSTM was introduced. The LSTM has the targeted catheter tip displacement (with respect to its straight configuration) as input and the required pressure as output. Therefore, the LSTM-based controller predicts directly the pressure needed to control the catheter despite hysteresis and obstacles. The predicted pressure is sent to the catheter in a feedforward manner. The number of neurons in each cell was set to 128. Adaptive Moment Estimation (Adam) and L2 loss are chosen as optimizer and loss function, respectively. The training and validation sets are partitioned in a ratio of 70% and 30%. The remaining hyperparameters of the LSTM are listed in Table I. The neural network was implemented based on PyTorch, an open source machine learning library. The training of the LSTMs were executed on an 4 GB NVIDIA® CUDA-capable GPU. Both LSTMs were trained for 100 epochs until they were adequately optimized. The whole training duration was around 20 to 30 minutes.

IV. EXPERIMENTAL VALIDATION

A. Validation of the f-LSTM and the c-LSTM under Different situations

The f-LSTM and the c-LSTM were tested with contact and non-contact case separately. This produced four sets of experiments in total. The catheter distal tip was controlled to follow an unseen descending sinusoidal trajectory as described in (2) with A = 8:

$$d(t) = e^{-0.1t}(A\sin(0.5\pi t - \pi/2) + A) \qquad [\text{mm}] \qquad (2)$$

The Maximum Absolute Error (MAE) and the Root Mean Square Error (RMSE) were used to evaluate the performance of the controllers. For each test trajectory, the validation procedure was repeated five times. The standard deviation of

TABLE II

THE MAE AND RMSE OF THE FREE SPACE LSTM AND CONSTRAINED SPACE LSTM IN FIVE TRIALS

	training environment	free-space							constrained-space						
test environment	metrics	1	2	3	4	5	mean	std	1	2	3	4	5	mean	std
free-space	MAE (mm)	1.50	1.23	1.15	1.21	1.19	1.26	0.12	9.92	9.88	9.81	9.85	9.69	9.83	0.08
	RMSE (mm)	0.43	0.40	0.41	0.44	0.45	0.43	0.02	2.84	2.82	2.80	2.83	2.74	2.81	0.04
constrained -space	MAE (mm)	4.87	4.85	4.89	4.89	4.93	4.89	0.03	1.89	2.05	2.04	1.99	2.05	2.00	0.06
	RMSE (mm)	1.72	1.72	1.74	1.72	1.76	1.73	0.02	0.32	0.40	0.39	0.36	0.38	0.37	0.03

the two metrics was also calculated to assess the repeatability of this experiment.

The results of five trials are detailed in Table II, while Fig. 4 shows one out of five trials. The f-LSTM could generally track the desired trajectory in the free case (see Fig. 4), with an average RMSE of 0.43 mm (see Table II). The maximun error occured at the beginning of the loading phase when the f-LSTM needs to compensate for the deadzone. It is shown that the c-LSTM also achieves good performance in the presence of obstacles, with an average RMSE of 0.37 mm (see Table II). The small standard deviations of the two experiments (0.02 mm and 0.03 mm) imply a high reproducibility of the experiments. On the contrary, as can be seen from the bottom left and top right subfigures in Fig. 4, the transferability across contact situations is limited. An LSTM trained in a certain situation performs poor when operating in another situation. When the f-LSTM is used in the presence of obstacles, the MAE rises to 4.89 mm and RMSE to 1.73 mm (see Table II). The RMSE in this is about four times higher than that of the f-LSTM tested in free space. Similarly, the c-LSTM also did not perform well when tested in free space. This highlights the importance of foreseeing a means to estimate the contact location and switch the system accordingly. The air pressure (control commands) that are predicted by both LSTMs in the free case are shown in Fig. 5. The figure shows how the c-LSTM overestimates the pressure compared to the f-LSTM, thus leading to a larger MAE (9.83 mm) and RMSE (2.81 mm) (see Table II).

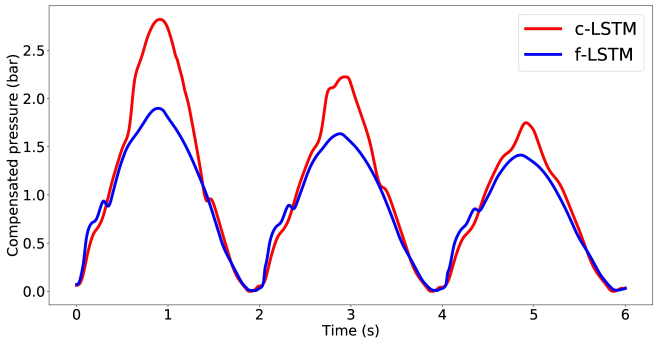

Fig. 5. The pressure predicted by both LSTMs in the free space case. The c-LSTM over-estimates pressure and is less suitable for use in a free space.

In cardiovascular applications, the required precision that clinicians indicate as being acceptable is typically in the order of 1–3 mm [25]–[27]. The obtained performance of the LSTM, when tested in the same case as it was trained, shows a good potential to satisfy this requirement. If contact states alter, the performance of the same LSTM will be insufficient.

B. Exploration of the Acceptable Working Range of a c-LSTM

Based on previous experiments one can expect that a c-LSTM trained for a given contact situation can only achieve an acceptable accuracy within a certain range around that location. Therefore, this section investigates in which range the c-LSTM could work. With the results of this study, one could then determine how many c-LSTMs need to be trained over the entire length of the catheter in order to allow a pre-defined required precision independent of contact state. The MAE and RMSE are used as the evaluation metrics for the control experiment. According to the precision requirement in clinical scenarios [25]–[27], a target of MAE $\leq$ 3 mm and RMSE $\leq$ 2 mm was set.

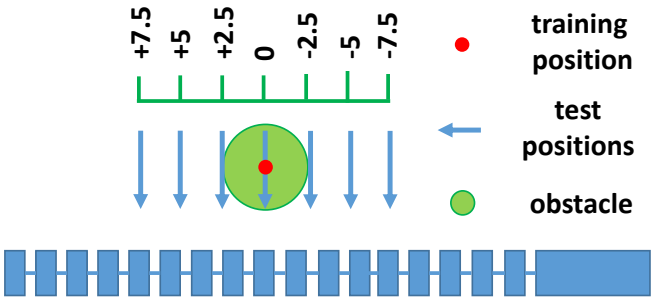

Fig. 6. c-LSTM tested at 7 different positions spaced at 2.5mm including the central position for which it was trained.

The experimental procedure that has been followed is shown in Fig. 6. As mentioned above, the c-LSTM was trained with the data collected when the obstacle was placed in the middle point of the catheter length. Afterwards, the obstacle was placed at 7 different positions separated at 2.5 mm distance. Three positions towards the end of the catheter distal tip are marked as positive, three towards the catheter base are marked as negative. Next, the catheter was controlled to follow a trajectory in (2) with A = 7 under the environmental contact. For each test position the experiment was repeated five times.

The results of the trajectory following experiments at different test positions are displayed in Fig. 7. The number in the upper left corner of each subplot represents the position of the obstacle (see Fig. 6) during the experiment. When the obstacle is more distal than during training, the c-LSTM trained in the midpoint usually underestimates the pressure. Fig. 7 clearly shows the performance decrease as the distance between the obstacle and the training position increases. When the obstacle moves from 0 to +7.5 mm, the RMSE of the c-LSTM increases from 0.33 mm to 1.65 mm, and the MAE rises from 1.15 mm to 3.21 mm. The performance

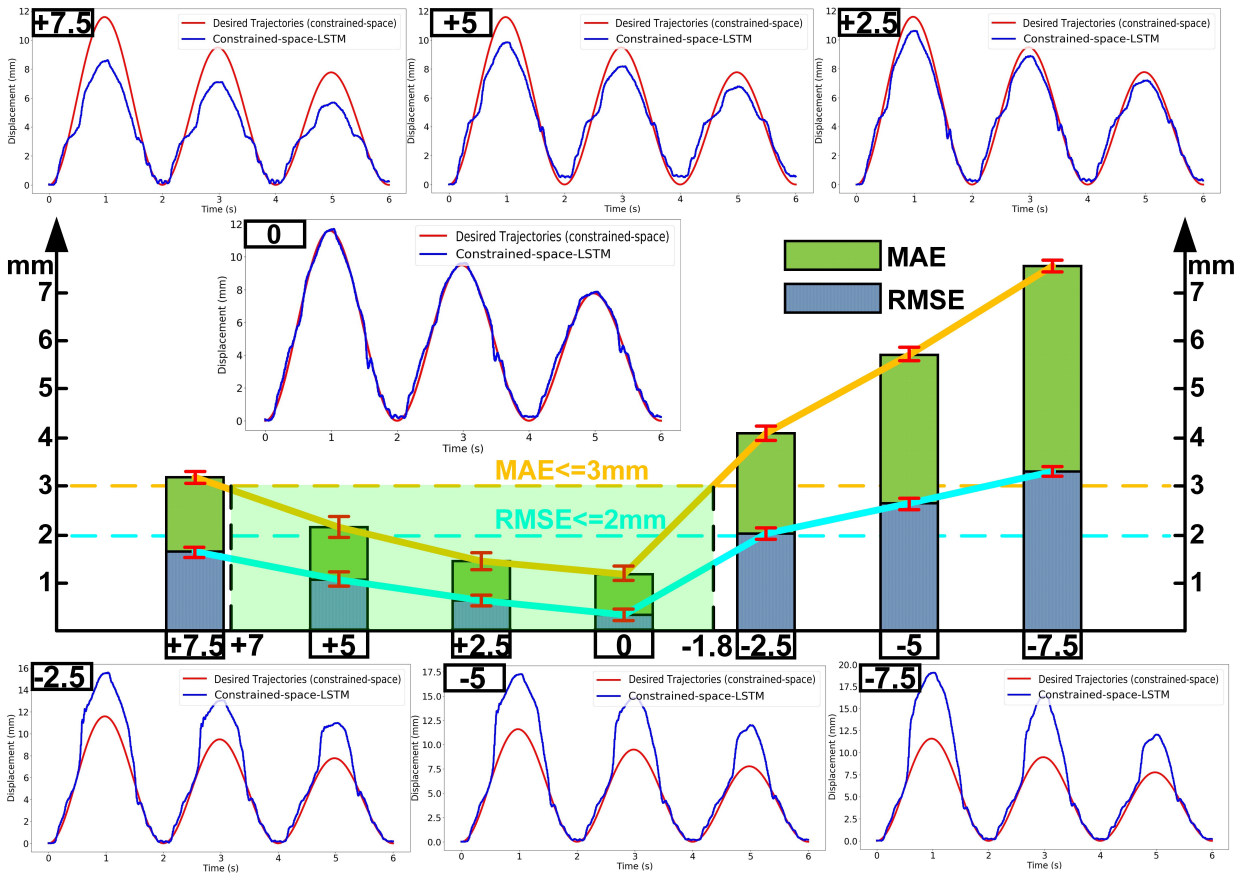

Fig. 7. The performance of the c-LSTM at different test positions shown in 7 subplots with each time test positions labeled on the top left corner (corresponding to the horizontal aixs of the bar plot). The bar plot reveals the average RMSE and MAE as well as their standard deviations.

degradation is more outspoken when the contact moves in the negative direction. Even though the c-LSTM can track the desired trajectory with high precision in the free motion part before catheter contact with the obstacle, it clearly over-compensates around the peak. From 0 to -7.5 mm, the RMSE of the c-LSTM increases from 0.33 mm to 3.33 mm, while the MAE grows from 1.15 mm to 7.63 mm. The results show a correlation between the performance of the c-LSTM and the location of the obstacle. By interpolation the results one can try to infer the performance of the c-LSTM at other locations between + 7.5 mm and -7.5 mm. Considering our pre-set goal, i.e. RMSE $\leq$ 2 mm and MAE $\leq$ 3 mm, it can be concluded that the c-LSTM can satisfy the accuracy requirements in the range of +7 mm to - 1.8 mm around the trained location. Since the length of our catheter is 77 mm, one can expect to need to train nine c-LSTMs with a distance separation of 8.8 mm in order to meet the overall control precision requirement.

V. CONCLUSIONS AND FUTURE WORK

A framework was proposed in this work to implement precise catheter control under environmental contact and hysteresis in the actuation system by using LSTMs. The framework proposes to train a single f-LSTM and a plurality of c-LSTMs. Depending on the required positioning precision, the different LSTMs are then to be switched. The contact status and position could be estimated by a shape sensing method e.g. based on FBGs but this part does not fall into the work of this paper.

Both LSTMs were validated on a fluidics-driven catheter segment. The first experiment verified the need to train multiple LSTMs. The experimental results indicate that both f-LSTM and c-LSTM could achieve good performance when tested in the same position, while their performance reduces when tested in a different contact situation. A second experiment explored the acceptable working range of a c-LSTM. It was shown that the acceptable working range of a c-LSTM in this work amounts to 8.8 mm. Within this range, the MAE and RMSE predicted by the LSTM are below 3 mm and 2 mm, respectively. Based on these results, it becomes possible to optimize the number and distribution of c-LSTMs over the entire length of the catheter. Considering that the time to train one LSTM is 20-30 minutes, it is feasible to train multiple LSTMs for precisely controlling the catheters, but training may become quite long for general cases.

In the future, we will extend this work to a two degrees-of-freedom (DOFs) robotic catheter and link this to real-time contact estimation based on FBG shape sensing.

ACKNOWLEDGEMENTS

This work was supported by the ATLAS project. ATLAS received funding from the European Union's Horizon 2020 research and innovation programme under the Marie Sklodowska-Curie grant agreement No. 813782.

REFERENCES

[1] P. S. Douglas, U. Hoffmann, M. R. Patel, D. B. Mark, H. R. Al-Khalidi, B. Cavanaugh, J. Cole, R. J. Dolor, C. B. Fordyce, M. Huang, M. A. Khan, A. S. Kosinski, M. W. Krucoff, V. Malhotra, M. H. Picard, J. E. Udelson, E. J. Velazquez, E. Yow, L. S. Cooper, and K. L. Lee, "Outcomes of anatomical versus functional testing for coronary artery disease," *New England Journal of Medicine*, vol. 372, no. 14, 2015.

[2] C. Li, X. Gu, and H. Ren, "A cable-driven flexible robotic grasper with lego-like modular and reconfigurable joints," *IEEE/ASME Transactions on Mechatronics*, vol. 22, no. 6, pp. 2757–2767, 2017.

[3] E. Bryn Pitt, D. B. Comber, Y. Chen, J. S. Neimat, R. J. Webster, and E. J. Barth, "Follow-the-leader deployment of steerable needles using a magnetic resonance-compatible robot with stepper actuators," *Journal of Medical Devices*, vol. 10, no. 2, 2016.

[4] J. Guo, Y. Liu, Q. Qiu, J. Huang, C. Liu, Z. Cao, and Y. Chen, "A novel robotic guidance system with eye-gaze tracking control for needle-based interventions," *IEEE Transactions on Cognitive and Developmental Systems*, vol. 13, no. 1, pp. 179–188, 2019.

[5] A. J. Chiluisa, F. J. Van Rossum, J. B. Gafford, R. F. Labadie, R. J. Webster, and L. Fichera, "Computational optimization of notch spacing for a transnasal ear endoscopy continuum robot," in *2020 International Symposium on Medical Robotics (ISMR)*. IEEE, 2020, pp. 188–194.

[6] G. Li, N. A. Patel, J. Hagemeister, J. Yan, D. Wu, K. Sharma, K. Cleary, and I. Iordachita, "Body-mounted robotic assistant for mri-guided low back pain injection," *International journal of computer assisted radiology and surgery*, vol. 15, no. 2, pp. 321–331, 2020.

[7] Y. Chen, L. Wang, K. Galloway, I. Godage, N. Simaan, and E. Barth, "Modal-based kinematics and contact detection of soft robots," *Soft Robotics*, vol. 8, no. 3, 2021.

[8] H. Tanabe, N. Takemura, H. Terao, H. Hagiwara, Y. Zushi, R. Murayama, M. Abe-Doi, and H. Sanada, "Vascular endothelium damage from catheter-induced mechanical stimulation causes catheter sleeve formation in a rabbit model," *Journal of Vascular Access*, vol. 21, no. 3, 2020.

[9] D. Wu, Y. Zhang, M. Ourak, K. Niu, J. Dankelman, and E. B. V. Poorten, "Hysteresis modeling of robotic catheters based on long short-term memory network for improved environment reconstruction," *IEEE Robotics and Automation Letters*, vol. 6, no. 2, pp. 2106–2113, 2021.

[10] D. Wu, M. Ourak, M. A. Ahmad, G. Borghesan, J. Dankelman, and E. Vander Poorten, "Feasibility of using a long short-term memory network for robotic catheter control," in *10 th Conference on New Technologies for Computer and Robot Assisted Surgery, Date: 2020/09/28-2020/09/30, Location: Barcelona, Spain*, 2020, pp. 68–69.

[11] R. S. Penning, J. Jung, N. J. Ferrier, and M. R. Zinn, "An evaluation of closed-loop control options for continuum manipulators," in *2012 IEEE International Conference on Robotics and Automation*. IEEE, 2012, pp. 5392–5397.

[12] P. Qi, H. Liu, L. Seneviratne, and K. Althoefer, "Towards kinematic modeling of a multi-dof tendon driven robotic catheter," in *2014 36th*

[18] Q. Qiao, G. Borghesan, J. D. Schutter, and E. B. Poorten, "Force from shape - estimating the location and magnitude of the external force on flexible instruments," *IEEE Transactions on Robotics*, vol. 37, no. 5, 2021.

Annual International Conference of the IEEE Engineering in Medicine and Biology Society. IEEE, 2014, pp. 3009–3012.

[13] P. Qi, C. Liu, A. Ataka, H. K. Lam, and K. Althoefer, "Kinematic control of continuum manipulators using a fuzzy-model-based approach," *IEEE Transactions on Industrial Electronics*, vol. 63, no. 8, 2016.

[14] S. B. Kesner and R. D. Howe, "Position control of motion compensation cardiac catheters," *IEEE Transactions on Robotics*, vol. 27, no. 6, 2011.

[15] J. Back, L. Lindenroth, K. Rhode, and H. Liu, "Model-free position control for cardiac ablation catheter steering using electromagnetic position tracking and tension feedback," *Frontiers Robotics AI*, vol. 4, no. MAY, 2017.

[16] W. Xu, J. Chen, H. Y. Lau, and H. Ren, "Data-driven methods towards learning the highly nonlinear inverse kinematics of tendon-driven surgical manipulators," *The International Journal of Medical Robotics and Computer Assisted Surgery*, vol. 13, no. 3, p. e1774, 2017.

[17] B. Yu, J. D. G. Fernández, and T. Tan, "Probabilistic kinematic model of a robotic catheter for 3d position control," *Soft Robotics*, vol. 6, no. 2, pp. 184–194, 2019.

[19] F. Khan, R. J. Roesthuis, and S. Misra, "Force sensing in continuum manipulators using fiber bragg grating sensors," in *2017 IEEE/RSJ International Conference on Intelligent Robots and Systems (IROS)*. IEEE, 2017, pp. 2531–2536.

[20] S. K. Sahu, C. Sozer, B. Rosa, I. Tamadon, P. Renaud, and A. Menciassi, "Shape reconstruction processes for interventional application devices: State of the art, progress, and future directions," *Frontiers in Robotics and AI*, vol. 8, 2021.

[21] X. T. Ha, M. Ourak, O. Al-Ahmad, D. Wu, G. Borghesan, A. Menciassi, and E. Vander Poorten, "Robust catheter tracking by fusing electromagnetic tracking, fiber bragg grating and sparse fluoroscopic images," *IEEE Sensors Journal*, vol. 21, no. 20, pp. 23 422–23 434, 2021.

[22] M. Azizkhani, I. S. Godage, and Y. Chen, "Dynamic control of soft robotic arm: A simulation study," *IEEE Robotics and Automation Letters*, 2022.

[23] M. De Volder, A. Moers, and D. Reynaerts, "Fabrication and control of miniature mckibben actuators," *Sensors and Actuators A: Physical*, vol. 166, no. 1, pp. 111–116, 2011.

[24] S. Hochreiter and J. Schmidhuber, "Long short-term memory," *Neural computation*, vol. 9, no. 8, pp. 1735–1780, 1997.

[25] H. Nijland, J. G. Gerbers, S. K. Bulstra, J. Overbosch, M. Stevens, and P. C. Jutte, "Evaluation of accuracy and precision of ctguidance in radiofrequency ablation for osteoid osteoma in 86 patients," *PLoS ONE*, vol. 12, no. 4, 4 2017.

[26] F. Bourier, T. Reents, S. Ammar-Busch, A. Buiatti, C. Grebmer, M. Telishevska, A. Brkic, V. Semmler, C. Lennerz, B. Kaess, M. Kottmaier, C. Kolb, I. Deisenhofer, and G. Hessling, "Sensor-based electromagnetic navigation (mediguide®): How accurate is it? a phantom model study," *Journal of Cardiovascular Electrophysiology*, vol. 26, no. 10, 2015.

[27] O. Al-Ahmad, M. Ourak, J. V. Roosbroeck, J. Vlekken, and E. V. Poorten, "Improved fbg-based shape sensing methods for vascular catheterization treatment," *IEEE Robotics and Automation Letters*, vol. 5, no. 3, pp. 4687–4694, 2020.